International Journal of Greenhouse Gas Control 94 (2020) 102896

Contents lists available at ScienceDirect

International Journal of Greenhouse Gas Control

journal homepage: www.elsevier.com/locate/ijggc

Novel ductile wellbore cementitious composite for geologic CO_2 storage

Jubilee T. Adeoye, Duo Zhang, Victor C. Li, Brian R. Ellis*

Department of Civil and Environmental Engineering, University of Michigan, United States

ARTICLE INFO

Keywords:
Geologic CO_2 storage
wellbore cement sheath
Mechanical integrity
CO_2 leakage mitigation
Engineered cementitious composite

ABSTRACT

CO_2 leakage through damaged wellbore cement sheaths is a major risk of geologic CO_2 storage (GCS), as conventional wellbore cement is brittle and can be damaged due to acid attack and downhole stresses during CO_2 injection. Here we examine a novel fiber-reinforced engineered cementitious composite (ECC) proposed as a substitute to conventional wellbore cement due to its superior ductility and intrinsic crack width control. ECC and conventional wellbore cement coupons were exposed to water in equilibrium with CO_2 at 50 °C and 10 MPa. The samples were retrieved after several days and their mechanical performance was evaluated using a four-point bending test, microhardness, and compressive strength analyses. Optical microscopy and mercury intrusion porosimetry were used to characterize the progression of the carbonation front and pore structures of the specimens. Control experiments were conducted under the same temperature and pressure conditions but with a N_2 headspace to isolate the impact of CO_2. It was found that carbonation increased the ultimate flexural strength of ECC but decreased its ductility. However, the ductility of carbonated ECC remained higher than that of conventional wellbore cements that exhibited brittle failure under all test conditions. Additionally, ECC exhibited minimal material loss and continued resistance to deformation in comparison to conventional wellbore cements. This suggests that while the exposure of ECC to CO_2 will alter its mechanical properties, altered ECC will continue to exhibit mechanical performance superior to conventional wellbore cement, and therefore shows promise as a highly durable wellbore cementing material for GCS applications.

1. Introduction

Geologic CO_2 storage (GCS) has been identified as a bridging technology to slow global climate change due to its ability to stabilize the atmospheric concentration of CO_2 by eliminating large streams of the greenhouse gas (IPCC and Metz, 2005). However, leakage of stored CO_2 from geologic reservoirs through damaged or abandoned wells remains a major risk of adopting GCS as a long-term strategy to slow global climate change (Bachu and Celia, 2009; Chow et al., 2003; Deel, 2007; Nordbotten et al., 2009, 2005; Watson and Bachu, 2009). Wellbore pathways through which CO_2 can leak from geologic reservoirs have been well documented, and include fractured cement sheaths, damaged steel casing, and steel casing/cement and cement/formation annular gaps (Bachu and Celia, 2009; Carroll et al., 2016). In particular, leakage of CO_2 through fractured cement sheaths is a major concern as conventional wellbore cementing materials are made of Portland cement, a brittle material that can be damaged by stresses generated during CO_2 injection and cyclic thermal swings (Nelson, 1990; Roy et al., 2018).

Previous studies that investigated the long-term effect of exposing wellbore cement to CO_2 have shown that the risks of cement sheath damage increase following carbonation and the overall mechanical strength of cement will be compromised following exposure to CO_2 under GCS conditions (Barlet-Gouédard et al., 2007; Fabbri et al., 2009; Li et al., 2015). Barlet-Gouédard et al. (2007) reported a 65% and 30% loss of bulk compressive strength in Portland cement exposed to CO_2-acidified water and wet supercritical CO_2, respectively, for six weeks at temperature and pressure conditions of 90 °C and 28 MPa. The exposure of the cement to CO_2 also led to damage and degradation characterized by spalling and cracking. In the study carried out by Li et al. (2015) on Portland cement coupons exposed to CO_2-acidified brine at temperature and pressure conditions of 95 °C and 10 MPa, three-point bending test and nanoindentation analysis were carried out on the coupons to investigate the effect of CO_2 on both the overall flexural and microstructural strength of the cement. Significant reduction in the overall flexural strength and modulus of elasticity was observed in samples exposed to CO_2 in comparison to control samples exposed to nitrogen headspace under similar temperature and pressure conditions. Fabbri et al. (2009) reported deterioration of the in-situ hydro-mechanical properties of Portland cement cores after several weeks of exposure to CO_2 at temperature and pressure conditions of 90 °C and 28 MPa. This alteration led to an increase in the permeability of the cement cores,

* Corresponding author.
E-mail address: brellis@umich.edu (B.R. Ellis).

https://doi.org/10.1016/j.ijggc.2019.102896
Received 15 June 2019; Received in revised form 31 October 2019; Accepted 3 November 2019

potentially increasing the risk of CO_2 leakage. Because the integrity of wellbore cement sheath is crucial for CO_2 storage security during GCS, there is a need to ensure that materials used in wellbore cementing can withstand the cyclic stresses induced during CO_2 injection, which are variable but can be in excess of 25 MPa (Jen et al., 2017; Rutqvist et al., 2007), and limit the extent of cement sheath damage under such conditions.

Engineered cementitious composite (ECC), a class of fiber-reinforced cementitious composites, is being proposed here as a possible candidate for wellbore cementing during GCS. ECC exhibits high tensile ductility, which is the capacity to undergo large tensile deformations before rupture, instead of brittle failure observed in conventional wellbore cement. ECC also shows strain-hardening behavior, which is the ability to bare more load at higher deformation through forming multiple fine cracks, typically less than 60 μm, at the microscale (Kan et al., 2010; Li, 2003). Studies have shown that ECC has a tensile strain capacity in the range of 2 to 5%, which is 200 to 500 times that of Portland cement and concrete (Li, 2009, 2003). Because tight cracks in conventional wellbore cement have been shown to heal autogenously when in contact with CO_2-rich fluids (Cao et al., 2015; Carroll et al., 2016; Huerta et al., 2016) in comparison to larger cracks, the ability of ECC to maintain cracks typically less than 60 μm during the stain hardening stage makes it an attractive candidate for wellbore cementing applications during GCS.

In a recent study carried out by Adeoye et al. (2019) on conventional M45 ECC exposed to CO_2-saturated water at P_{CO2} of 10 MPa and temperature of 50 °C, an increase in microhardness was observed in all regions of the composite following reaction with CO_2. The increase in hardness was attributed to pore refinement in the ECC matrix, due to continuous pozzolanic reactions, and reworking of parent cementitious material into a denser matrix following carbonation. Such pore refinement and reworked matrix has been reported by Cheshire et al. (2017) in cement cores recovered from an injection well in a CO_2-enhanced oil recovery field in West Texas, and can improve the resistance of the material to deformation and reduce fluid permeability through the composite. Adeoye et al. (2019) also observed that the fiber/matrix interfacial transition zone (ITZ) in the M45 ECC was densified with reaction products that were identified as calcium carbonate after exposure to CO_2. Such densification of the ITZ could impact the ductility, long-term strain hardening property, and multiple cracking behavior of ECC, as the denser ITZ will increase the bonding between fibers and matrix, potentially promoting rupturing of fibers rather than pull out under tensile stress (Li et al., 2002; Li, 2003; Redon et al., 2001). To determine the suitability of ECC as substitute for conventional wellbore cementing materials in injection wells during GCS, it is important to understand how the ductility and mechanical integrity of ECC will be impacted by reaction with CO_2 under typical GCS conditions.

This work investigates the changes in the mechanical properties of an ECC material formulated for wellbore cementing applications in order to predict its long-term integrity following exposure to CO_2 under typical GCS conditions. A series of static batch experiments were carried out, simulating diffusive mass flow conditions expected in wellbore cement sheath, and a four-point flexural test was used to determine the impact of CO_2 on the ductility of ECC in comparison to conventional wellbore cements. The evolution of ECC microstructure was also characterized to provide insight regarding the factors that will impact the overall mechanical performance of ECC during GCS.

2. Materials and methods

2.1. Material selection

ECC material selection was carried out to achieve a fresh state mix with flow properties that are more representative of a wellbore cement slurry in comparison to standard M45 ECC (See Supporting Information) (Guillot, 1990; Li, 2009; Nelson et al., 1990). Silica sand used in standard M45 ECC was replaced with low calcium content Class F fly ash (ASTM C618, Type F) to improve the flowability of the mix in the fresh state. The chemical composition of the fly ash used is presented in Table 1. Type III cement, which is early-strength cement, was used for the ECC mix instead of Class H wellbore cement to compensate for the negative effect of high fly ash content and water to cement ratio on early-age strength development. Type III cement is able to develop early-age strength faster than Class H wellbore cement because of its higher surface area (5000 m^2/kg) in comparison to Class H wellbore cement (1600 m^2/kg) and higher Al-phase content (Michaux et al., 1990). A fly ash: cement ratio of 50:50 by weight, which is a typical wellbore comment slurry blend, was used for specimen preparation in this study (Nelson et al., 1990). REC 15 polyvinyl alcohol (PVA) fiber with a length of 8 mm and 0.5% oil coating supplied by Kuraray Ltd. (Japan) was chosen over the 12 mm fiber used in standard M45 ECC because shorter fibers promote more uniform fiber dispersion in a low-viscosity mix. The physical and mechanical properties of the PVA fibers are presented in Table 2. In this study, we have used a 1.1% fiber volume, which is considerably less than the 2% fiber volume used in conventional ECC (Li, 2009). This is because the lower volume promoted uniform dispersion of fibers in the slurry. Anti-settling agent was added to prevent free water by promoting gelation in the fresh mixture and dispersant was added for viscosity control. Samples were mixed using tap water. For the sake of brevity, this version of ECC is labeled in this paper as WECC (wellbore ECC). Reference samples representing conventional wellbore cement were prepared using Class H cement.

Table 1
Chemical composition of fly ash.

Chemical Composition.	SiO_2	Al_2O_3	Fe_2O_3	SO_3	CaO	MgO	Na_2O	K_2O	LOI[a]
%	51.8	20.6	14.8	0.8	4.1	1.0	1.3	2.4	2.80

[a] LOI is loss on ignition.

2.2. Sample preparation

Three sets of samples were prepared with the mix proportions presented in Table 3. WECC represents the composition of ECC proposed for wellbore cementing applications during GCS. Fiber-free WECC (hereafter referred to as FFWECC) has the same composition as WECC, but the fibers have been excluded from the mix to isolate the unique impact of the fibers on the microstructural behavior of WECC under GCS conditions. Thus, FFWECC is comparable to conventional fly ash-amended wellbore cement (Kutchko et al., 2009; Zhang et al., 2014). Class H composition is the conventional wellbore cementing material (Nelson et al., 1990). Both FFWECC and Class H served as benchmarks to evaluate the mechanical performance of WECC.

For WECC, the solid components were dry-mixed at 200 rpm for 5 min. A premixed solution containing the liquid components was then added to the mix over the course of 5 min. Subsequently, PVA fibers were added to the slurry over a period of 2.5 min, mixed at a constant rate of 200 rpm. The slurry was further mixed after the addition of the fibers for an additional 2.5 min, to ensure uniform fiber dispersion. FFWECC was prepared using a similar approach as WECC, but the fiber addition process was excluded. For Class H cement, the cement was mixed for 3 min followed by the ddition of the premixed liquid components for 5 min. All samples were prepared using a 6-liter countertop mixer (KitchenAid). The fresh slurries were cast in customized Plexiglas rectangular coupon molds (102 mm x 34 mm x 10 mm) shown in Fig. 1a to generate several specimens for flexural testing, and in 2-inch cubic molds prepared according to ASTM standard C109 for compressive strength analysis of cement mortars (ASTM, 2016). The specimens were placed in a curing chamber (Temp. = 22 ± 2 °C and RH = 99 ± 1%) and demolded 24 hours after casting. The samples were then cured

Table 2
Physical and mechanical properties of PVA fibers used in WECC.

Length (mm)	Diameter (μm)	Density (kg/m^3)	Tensile strength (MPa)	Elongation (%)	Young's Modulus (GPa)
8	39	1.3	1600	7	42

Table 3
Composition of materials. Water content is reported as a fraction of the total solid weight WCEE: wellbore ECC; FFWECC: fiber-free WECC; Class H: conventional wellbore cement.

Sample Type	Solid Phase		Liquid Phase	Fiber vol. (%)
	Cement	Fly ash	Water	
WECC	0.5	0.5	0.45	1.1
FFWECC	0.5	0.5	0.45	0
Class H	1	0	0.38	0

Note: Additives including dispersant, antifoam, and anti-settling agents were added to modify slurry fresh state flow properties. Table 3: Ultimate flexural strength (modulus of rupture) for specimens as a function of time.

under this condition for 28 days.

2.3. Static batch experiments

Eight WECC/FFWECC and six Class H cement samples were placed in 600 mL batch reactors filled with 300 mL of deionized water with a resistivity greater than 18.2 MΩ-cm such that the samples were fully submerged (Fig. 1b). Pure water was used in this study to ensure that the samples were exposed to the most acidic environment under the chosen temperature and P_{CO2} conditions (Rimmelé et al., 2008; Spycher and Pruess, 2005). The temperature and P_{CO2} in the batch reactors were subsequently elevated to 50 °C and 10 MPa, respectively. For WECC and FFWECC, two samples were retrieved from each reactor after 2, 7, 14, and 28 days, while Class H cement samples were retrieved after 2, 7, and 21 days. For each pair of samples retrieved from the reactor, the samples were replaced with two Teflon coupons of the same dimensions. This ensured a constant water level in the batch reactor throughout the experiment, such that the samples were completely submerged in water at all times, without needing to add additional water to the reactor. Similarly, two 2-inch cubic specimens of each sample type were exposed to CO_2-acidified water under the same temperature and pressure conditions and retrieved after 7 days of reaction.

To decouple the effect of elevated temperature and pressure conditions from the unique interactions between WECC and CO_2, a control experiment was set up in which the coupons were exposed similarly to an N_2 headspace with P_{N2} of 10 MPa and temperature of 50 °C. The headspace in the batch reactor was purged with nitrogen prior to starting the experiment to eliminate ambient air containing CO_2 from the reactor. After retrieving the samples from the reactor, they were air-dried at room temperature conditions (23 ± 2 °C) for 24 hours to expel surficial water before carrying out the four-point bending flexural test.

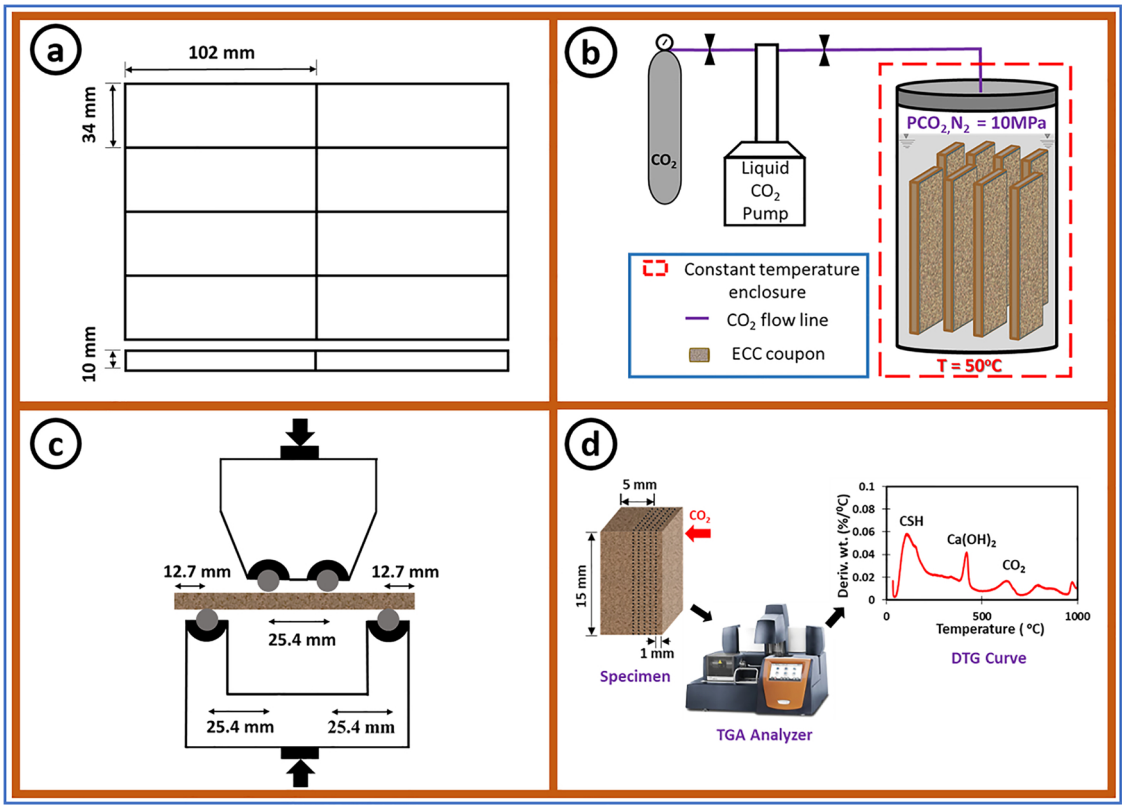

Fig. 1. Experimental procedures for the study. (a) Customized mold for coupon specimens. Dimensions were chosen to maintain a coupon span to height ratio of 10:1. (b) Experimental setup for the batch study. Temperature and pressure were kept constant throughout the study. Coupons specimens were replaced with dummy Teflon coupons after sample retrieval. (c) Customized setup for four-point bending test. Top and bottom sections of the test cell were cut out of a single piece aluminum block and steel dowels were used as rollers. (d) Flow diagram for TGA analysis.

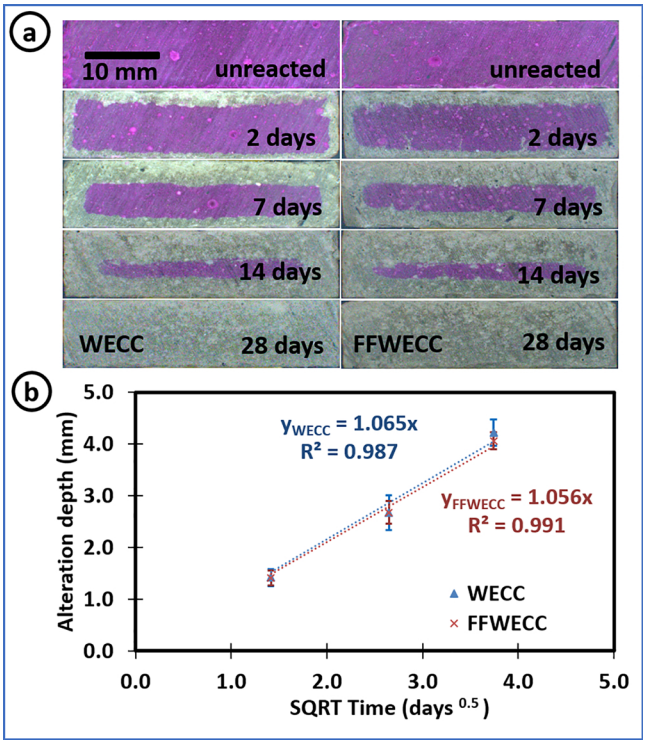

Fig. 2. (a) Alteration front of reacted and unreacted WECC and FFWECC specimens using phenolphthalein pH indicator. Pink and clear regions are the uncarbonated and carbonated regions of the samples, respectively. (b) The combined plot of the alteration depth vs. SQRT time for WECC and FFWECC using phenolphthalein pH indicator. Equations YWECC and YFFWECC describe the extent of carbonation for WECC and FFWECC, respectively, as a function of time using phenolphthalein pH indicator. Error bars represent the standard deviation of 10 measurements of the altered depth from the edge of the coupon to the leading edge of the alteration zone. The goodness of the linear fit of the alteration depth vs. square root (SQRT) of time indicates that CO_2 transport in WECC and FFWECC is a diffusion-controlled process.

2.4. Sample analysis

2.4.1. Four-point bending test

A four-point bending test was carried out to determine the ductility and ultimate flexural strength of the specimens, pre- and post-reaction with CO_2, using an Instron mechanical test frame equipped with Bluehill software (Instron) for actuator control and data acquisition. The sample stage was custom-made using single-piece aluminum frames for the upper and lower supports, with steel dowels used as rollers, as shown in Fig. 1**c.** The coupons were pre-loaded to 20 N and subsequently loaded at a constant displacement rate of 0.1 mm/min. The loading rate was maintained until the load dropped below 50% of the maximum load sustained by the sample. The flexural stress (σ_f) of the coupons was determined using the expression:

$$\sigma_f = \frac{Fl}{bd^2} \tag{1}$$

where F is the loading force (N), l is the distance between the two supporting pins (mm), b is the width of the coupon (mm), and d is the thickness of the sample (ASTM, 2012). The modulus of rupture (σ_{fmax}) was computed based on the peak value of F.

2.4.2. Microhardness and compressive strength analyses

Microhardness analysis was carried out to determine the variation in local micromechanical strength and resistance to deformation of the different regions of the sample following acid attack. Samples were polished using a series of finer sandpaper grit sizes with a final finish achieved using a P2400-grit sandpaper and the test was carried out using a Vickers hardness tester (LECO). The altered and unaltered regions of the coupons were segmented into different zones, with more data points obtained from the edge of the sample in contact with CO_2-acidified water (Adeoye et al., 2019; Zhang et al., 2014). This ensured a higher resolution of the microhardness measured along the most altered region of the core. The test used a loading force of 500 g and a dwell time of 10 seconds. The microhardness of each zone was reported as a hardness value (HV) for a 500 g load based on the average hardness of 12 indents, with higher HV indicating greater resistance of the material to deformation (Dieter and Bacon, 1986).

Compressive strength analysis was carried out on the carbonated and unaltered 2-inch cubes using a Forney compression machine (Forney). The initial load of 5 N was applied to the load cell and a constant loading rate of 3 N/s was applied until the peak load was attained. The test was stopped after the load dropped to 75% of the peak load. The compressive strength of the samples was then determined using the expression:

$$F_m = \frac{P}{A} \tag{2}$$

Where F_m is the compressive strength in MPa, P is the total maximum load in N, and A is the area of loaded surface mm^2 (ASTM, 2016).

2.4.3. Extent of carbonation alteration

To determine the extent of alteration and carbonation of the samples following reaction with CO_2, each coupon was sectioned using a saw and the sectioned surface was stained with phenolphthalein pH indicator to determine the carbonated and uncarbonated regions based on the variation in the pH along the reaction front. The depth of the altered zone was estimated by taking the average of 10 measurements from the edge of the coupon to the edge of the altered zone (i.e., region of reduced pH). To further compare the structural change and material loss along the edge of the sample following reaction with CO_2 in WECC and FFWECC, optical microscopy was carried out on the polished surface of the sectioned specimens using a Nikon LV100ND optical microscope (Nikon Instruments Inc.) equipped with a 5x magnification lens.

2.4.4. Mercury intrusion porosimetry

Quantitative changes in the porosity and pore size distribution of the specimens were determined using mercury intrusion porosimetry (MIP). Samples were cut into ~30 mm^3 sections and dewatered via solvent replacement by soaking in isopropanol for 7 days (Feldman, 1987; Gallé, 2001). Specimens were subsequently vacuum-dried in a desiccator at ambient temperature conditions for 72 hours. The samples were then analyzed in 5 cm^3 penetrometers using a MicroActive AutoPore V 9600 mercury intrusion porosimeter (Micromeritics Instrument Corporation) with maximum injection pressure of 421 MPa.

2.4.5. Thermogravimetric analysis

Thermogravimetric analysis (TGA) was used to quantify the hydrated products in WECC and FFWECC samples at different depths along the reaction front after exposure to CO_2 acidified water. This was done to investigate the differences in the evolution of WECC carbonation products relative to FFWECC and to chemically investigate if the fibers will alter the carbonation trends observed in conventional fly ash-amended wellbore cement. 15 mm x 5 mm x 10 mm sections of the coupons were obtained and each sample was sanded at 1 mm intervals along the reaction front toward the center of the coupon as described in Fig. 1d. The 1 mm section represents the section of the sample in direct contact with CO_2 acidified water. Samples were analyzed using a thermogravimetric analyzer (TA Instruments, SDT 650). 20 mg of each specimen was placed in a 90 µl aluminum crucible and the temperature was ramped up to 35 °C at a rate of 1 °C/min, and held constant for 60 min to eliminate free water (Neves Junior et al., 2019). The

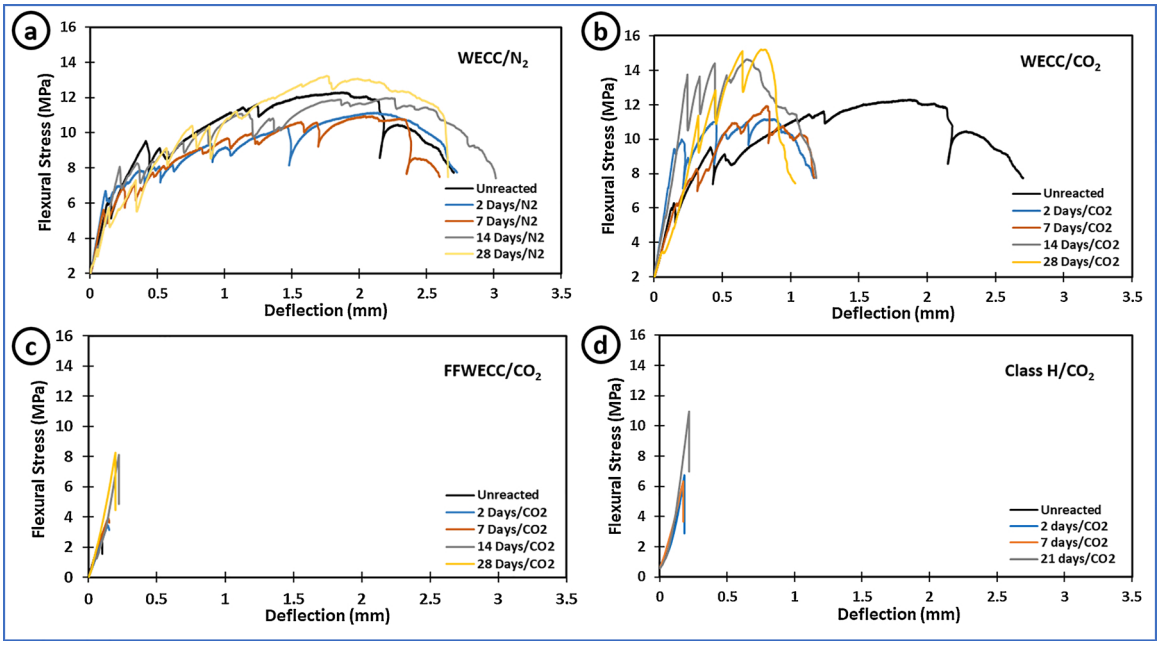

Fig. 3. Four-point flexural stress-deflection curves for (a) unaltered WECC and carbonated WECC coupons, (b) unaltered WECC and control WECC coupons exposed to N_2 headspace (c) unaltered and carbonated FFWECC coupons (d) unaltered and carbonated Class H coupons, under GCS conditions of 50 °C and 10 MPa.

temperature was subsequently ramped up to 1000 °C at a rate of 10 °C per minute.

3. Results and discussion

3.1. Long-term alteration of WECC

Fig. 2**a** presents the depth of carbonation at different time points for WECC and FFWECC, obtained by staining the cross-section of the specimens with phenolphthalein pH indicator before and after exposure to CO_2. The clear and pink regions of the stained surfaces represent the altered and unaltered sections of the coupons, respectively (RILEM, 1984; Verbeck, 1958; Zhang and Shao, 2016). The result indicates that the average depth of carbonation for WECC and FFWECC after two days of reaction was 1.42 ± 0.17 mm and 1.41 ± 0.15 mm, respectively. Both WECC and FFWECC samples were fully reacted after 28 days of reaction. The fact that the carbonation depths were comparable for both WECC and FFWECC at different time points suggests that the presence of fibers did not promote deeper penetration of CO_2 into the ECC matrix and will therefore not enhance the extent of carbonation under GCS conditions.

Fig. 2**b** plots alteration depth as a function of the square root of time, which describes the extent of carbonation according to Fick's second law of diffusion and is typically used to estimate the rate of carbonation of cement in systems under constant concentration boundary conditions (Neville, 2011). The results show that the early-time alteration of the WECC and FFWECC follow linear trends with $R_{WECC} = 0.98$ and $R_{FFWECC} = 0.99$ (Fig. 2b**)**. Based on this correlation, CO_2 penetration through WECC and FFWECC at different time points was shown to be a diffusive process according to:

$$Y_{WECC} = 1.065x \quad (3)$$

$$Y_{FFWECC} = 1.056x \quad (4)$$

where Y_{WECC}, Y_{FFWECC} are the depths of alteration in mm for ECC and FFWECC, respectively, and x is the square root of time in days$^{1/2}$. Based on equations (3) and (4), the estimated extent of carbonation for the WECC and FFWECC samples after 28 days of exposure to CO_2 acidified water will be 5.63 and 5.58 mm, respectively. This is consistent with the observation in the 28-day samples that showed that the 10 mm thick samples had been fully reacted, as the carbonation progressed from all sides of the rectangular specimens.

In contrast to the WECC and FFWECC samples in which significant carbonation was observed after reaction with CO_2, the Class H cement samples showed minimal carbonation that was limited to the edge of the coupons after 28 days of exposure to CO_2. This is attributed to the denser microstructure of Class H cement due to the absence of fly ash and lower water content in comparison to the WECC and FFWECC mixes (Kutchko et al., 2009; Lye et al., 2015; Zhang and Li, 2013).

3.2. Effect of carbonation on mechanical integrity of WECC

The four-point bending tests carried out on WECC specimens showed that the unreacted sample exhibited multiple microcracking behavior and significant ductility. The reaction of WECC specimens with CO_2 impacted the ductility of ECC negatively, while the ductility of control samples exposed to N_2 headspace under the same temperature and pressure conditions remained relatively unaltered over the same period.

Fig. 3**a** shows the stress-deflection curves as a function of time for WECC samples exposed to N_2 headspace. The unreacted WECC and all control samples exposed to N_2 headspace for 2, 7, 14, and 28 days showed deflections in the range of 2.2 to 2.5 mm at the maximum flexural stress and exhibited multiple cracking at the bottom surface of the coupons. The samples also showed a gradual decrease in stress relative to deflection, subsequent to achieving maximum flexural strength, which is typical in strain hardening ECC (Mohamed and Li, 1994) rather than a sudden drop to zero observed in brittle wellbore cement after achieving maximum flexural strength.

Fig. 3**b** shows the stress-deflection curves for WECC control samples exposed to CO_2 acidified water. In contrast to control samples exposed to N_2 headspace, carbonated WECC showed a significant decline in the total deflection of the specimens, with deflection in the range of 0.5 to 0.8 mm at the ultimate flexural stress. This deflection is approximately one-third of the deflection of control samples exposed to N_2 headspace. The carbonated samples also exhibited a rapid increase in stress relative to deflection characterized by the increase in the initial slope of the stress-deflection curve as the extent of carbonation increased. The

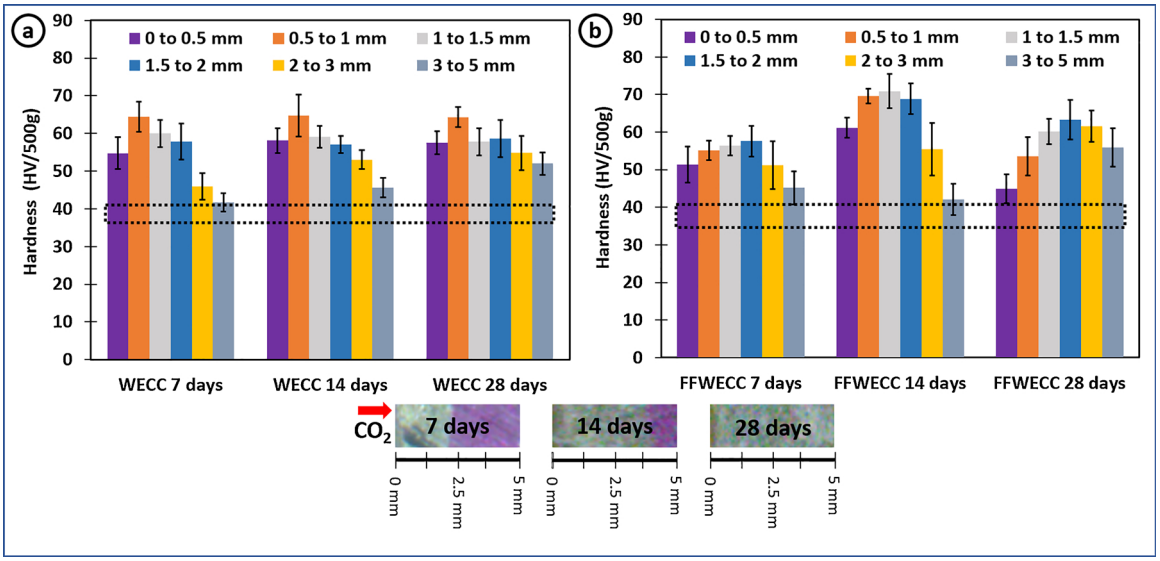

Fig. 4. Time-dependent evolution of microhardness for (a) WECC and (b) FFWECC samples, respectively, following exposure to CO_2 acidified water at 50 °C and 10 MPa P_{CO2} for 7, 14, and 28 days. The dotted lines in Fig. 4**a** and **b** represent the range of average hardness for uncarbonated WECC and FFWECC samples. Picture inserts at the bottom of the figure indicate the extent of post reaction alteration depth associated with both WECC and FFWECC samples revealed by phenolphthalein pH indicator.

significant decrease in ductility of WECC and rapid initial increase in stress relative to deflection after carbonation may be explained by stiffening and strengthening of the specimen by the combined effects of densification of the microstructure of WECC matrix, as reported by Wu et al. (2018), and densification of the fiber/matrix interfacial transition zone (ITZ) reported by Adeoye et al. (2019) following carbonation. In particular, the densified ITZ increases the interfacial bonding between the fiber and the matrix such that the fibers are unable to pullout easily from the matrix under flexural stress, leading to fiber rupture and subsequent embrittlement of the composite.

Fig. 3c and Fig. 3**d** show the stress-deflection curves of the FFWECC and Class H cement samples, respectively. In contrast to WECC, which exhibited strain hardening and ductility, FFWECC and Class H samples exhibited brittle failure prior to and after exposure to CO_2. Similar to WECC, we observed an increase in the ultimate flexural strength of FFWECC and Class H wellbore cement with increased extent of carbonation. The modulus of rupture increased from 2.9 to 8.2 MPa and 6.2 to 10.9 MPa after 28 and 21 days of reaction, for FFWECC and Class H cement, respectively.

Table 3 presents the ultimate flexural strength, known as the modulus of rupture, for each of the materials. It was observed that the ultimate flexural strength for WECC was consistently higher than that of FFWECC and Class H irrespective of the extent of carbonation of the material. Hence, while the carbonation reaction decreased the ductility of WECC, WECC continued to exhibit superior ductile performance in comparison to conventional wellbore cementing materials under typical GCS conditions. In addition, the superior ductility and multiple cracking behavior of the unaltered WECC (Fig. 3a) and WECC exposed to N_2 headspace (Fig. 3b) suggest that ECC can potentially be employed for wellbore cementing in other deep geologic environments such as in oil and gas wells, in the absence of CO_2, without deterioration of its long- term strain hardening properties.

3.3. Microhardness and resistance to deformation

Fig. 4a and Fig. 4**b** present hardness values for WECC and FFWECC specimens, respectively, pre- and post-reaction with CO_2. The results indicate that the resistance of WECC to deformation was not compromised following reaction with CO_2-acidified water in comparison to FFWECC. The average hardness of the WECC composite prior to carbonation was 37.9 ± 2.5 HV/500 g. A general increase in hardness, both at the carbonated edge and uncarbonated core of the sample, was observed following reaction with CO_2. The fact that the uncarbonated region exhibited an increase in hardness can be explained by the pore refinement due to continuous cement hydration under high temperature and pressure conditions (Adeoye et al., 2019; Kutchko et al., 2009; Zhang et al., 2014). For the carbonated region, the highest hardness value was observed in the 0.5 to 1.0 mm section of the specimen, indicating that the most substantial pore refinement due to carbonation occurred in this region. Although the WECC sample had been fully reacted after 28 days of reaction, the sample showed higher microhardness in comparison to the unaltered material, indicating that reaction with CO_2 did not negatively alter its resistance to deformation. For FFWECC samples, the average hardness of the material prior to reaction was 37.6 ± 3.0 HV/500 g, which was similar to the hardness of the unreacted WECC. Similar to WECC, a general increase in the hardness was observed at the core and edge of the FFWECC coupon compared to the unreacted material following exposure to CO_2.This is attributed to continuous coarsening of the matrix microstructure resulting from pozzolanic reactions under high temperature and pressure conditions (Adeoye et al., 2019; Zhang et al., 2013). While the WECC samples showed the highest hardness at the 0.5 to 1.0 mm zone of the coupon, the highest hardness values were measured in the 1.0 to 2.0 mm section of FFWECC coupons. This is likely due to greater extent of densification at the edge of the carbonated WECC, relative to the FFWECC specimens, due to the presence of the PVA fibers. At 28 days of exposure, the hardness of the FFWECC specimen was significantly lower at the edge of the coupon than the hardness of the samples exposed to CO_2 for 14 days. This is likely due to deterioration of material at the edge of the sample after prolonged exposure to the CO_2-acidified water. The fact that this sharp retrogression in hardness was not observed in WECC samples containing fibers suggests that the presence of fibers in WECC helped to maintain the structural stability of the material under the GCS conditions and may help maintain the integrity of the wellbore cement sheath following acid attack.

Fig. 5a and **b** show optical images of the edge along the transverse section of the unaltered FFWECC coupon and FFWECC coupon after 28 days of exposure to CO_2 acidified water, respectively, while Fig. 5**c** and **d** show optical images of the edge of the unreacted WECC coupon and WECC coupon after 28 days of exposure to CO_2 acidified water.

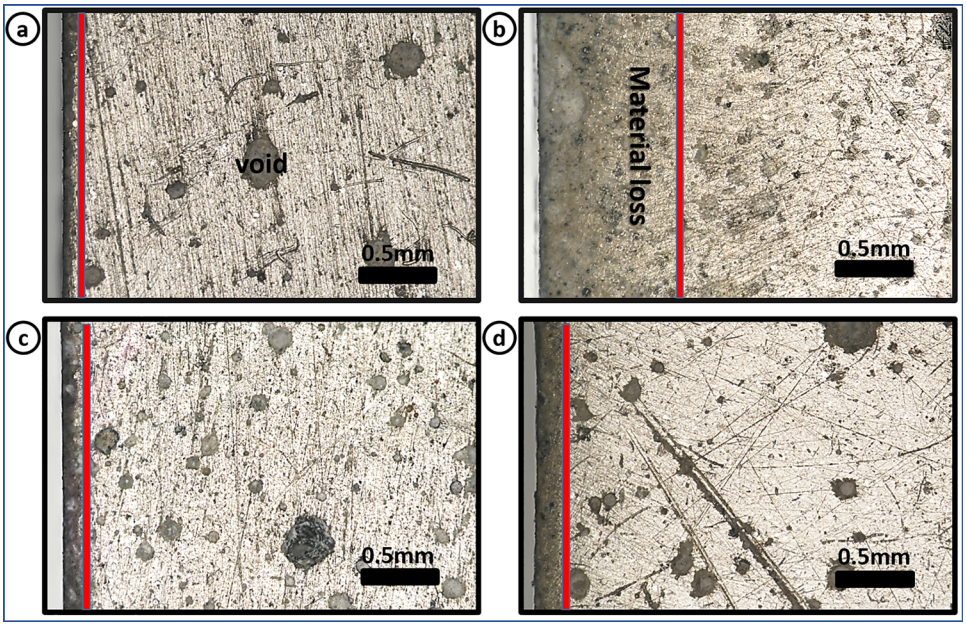

Fig. 5. Optical image of (a) unaltered FFWECC coupon (b) FFWECC coupon after exposure to CO_2 acidified water (c) unaltered WECC coupon, and (d) WECC coupon after exposure to CO_2 acidified water, at temperature and pressure conditions of 50 °C and 10 MPa.

Although minimal material loss was observed at the edge of WECC samples after 28 days of reaction **(**Fig. 5**d)** in comparison to the unreacted sample (Fig. 5c), there was significant material loss at the edge of the FFWECC specimens in comparison to the unreacted FFWECC sample. This is consistent with the surface microhardness result that showed a significant decrease in the hardness of the FFWECC samples after 28 days of reaction, supporting the hypothesis that the presence of the fibers promoted the long-term structural stability of the composite. This structural stability and absence of material loss in WECC relative to the FFWECC is imparted by the microfibers that helped to bind the matrix together, which will ensure the integrity of the cement sheath and promote secure storage during GCS.

3.4. Evolution of compressive strength

Table 4 presents the average compressive strength for WECC, FFWECC, and Class H samples at different time points and exposure conditions. In wellbore cementing, the development of early-age compressive strength of the cement ensures both structural support for the casing and zonal isolation of borehole intervals (Labibzadeh et al., 2010). The recommended compressive strength of wellbore cement after 24 hours is 3.5 MPa (500 psi) (Labibzadeh et al., 2010; Ridha et al., 2013). Meeting this target 24 hr compressive strength is crucial for wellbore cement design in order to limit the wait-on-cement time, i.e. the time between drilling operations, while ensuring the integrity of the cement job.

The results in Table 4 indicates that the compressive strengths of WECC and FFWECC were comparable after 24 hours of curing, although the compressive strength of the WECC was slightly higher (9.1 MPa) than FFWECC (8.1 MPa). Class H cement showed considerably higher compressive strength (13.3 MPa) than both WECC and FFWECC. After 28 days of curing, the compressive strength of all sample types increased significantly as expected, with WECC, FFWECC, and Class H having compressive strengths of 30, 26.2, and 47.9 MPa, respectively. The fact that the 24 hr and 28 day compressive strengths of WECC and FFWECC samples were consistently lower than that of Class H cement is due to the high volume of fly ash in WECC and FFWECC, up to 50% replacement by mass. Such high-volume substitution of cement with fly ash has been shown to reduce the overall compressive strength of Portland cement (Harison et al., 2014; Lam et al., 1998). Additionally, the WECC and FFWECC specimens contained a higher proportion of water (45% water:solid) in comparison to Class H specimens (38% water:solid).

Table 4
Compressive strength for WECC, FFWECC, and Class H sample carbonation at early-age, late-age, and post-carbonation.

Sample	24 hr unreacted	7 days unreacted	7 days carbonated	% post carbonation change
WECC	9.1	30.0	39.2	30.6
FFWECC	8.0	26.2	28.2	7.8
Class H	13.3	47.9	51.5	7.5

Following carbonation for 7 days, further increase in the compressive strength of the samples was observed indicating that carbonation of the samples under the temperature and pressure conditions tested did not compromise the compressive strength of the specimens. The increase in compressive strength can be linked to the further hydration and pore refinement of the cementitious materials under higher GCS temperatures and pressures. While the FFWCC and Class H showed approximately 8% increase in average compressive strength following carbonation, WECC showed a 30% increase in compressive strength. The difference between the increase in compressive strength for FFWECC and WECC can be linked to the strengthening of the WECC composite due to the densification of the fiber/matrix interface following carbonation, which improves the bonding between the fiber and the matrix and consequently the overall strength of the composite (Adeoye et al., 2019).

It is instructive to note that in addition to exhibiting a higher compressive strength performance in comparison to conventional fly ash amended wellbore cement, this study has shown that WECC exhibits superior flexural strength and ductility in comparison to FFWECC, furthering its potential as a candidate for wellbore cementing applications.

3.5. Evolution of WECC pore structure

The pore structure of wellbore cement can influence the transport of fluids through the uncracked material and thus impact its resistance to CO_2 attack. To reveal the evolution of WECC's pore structure in

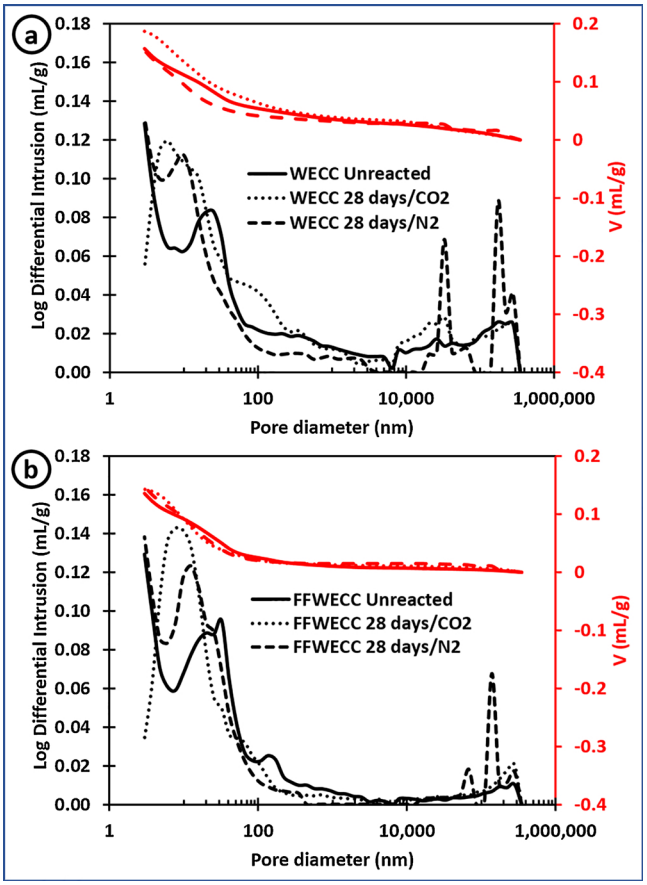

Fig. 6. Cumulative and differential pore size distribution for unreacted and altered (a) WECC and (b) FFWECC follow exposure to CO_2 acidified water and N_2 headspace for 28 days at temperature and pressure conditions of 50 °C and 10 MPa. The "critical diameter" corresponding pore diameter at the inflection point on the intrusion volume vs. pore diameter curve.

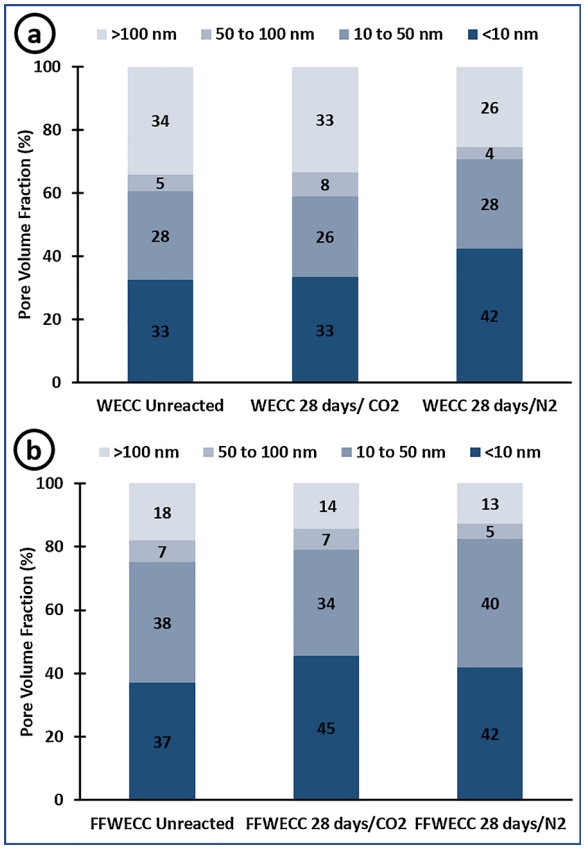

Fig. 7. Normalized pore volume fraction distribution for unreacted and altered (a) WECC and (b) FFWECC follow exposure to CO_2 acidified water and N_2 headspace for 28 days at temperature and pressure conditions of 50 °C and 10 MPa.

response to exposure to CO_2-acidified water, the pore size distribution curves obtained using MIP are plotted in Fig. 6a and **b** for WECC and FFWECC samples, respectively. As shown in Fig. 6**a**, the total intruded volume in WECC increased from 0.16 mL/g to 0.19 mL/g following 28 days of carbonation, whereas the total intruded volume for the control samples exposed to N_2 headspace remained relatively unchanged at 0.15 mL/g. In the absence of fiber, however, the conventional fly ash amended wellbore cementing material (FFWECC) showed comparable intruded volumes of approximately 0.14 mL/g for the unaltered and carbonated samples (see Fig. 6b). The total intruded volume for the control FFWECC sample exposed to N_2 headspace also remained constant at 0.14 mL/g after 28 days.

In Fig. 6, the "critical diameter" can be visually identified as the pore diameter at the maximum inflection point on the intrusion volume vs. pore diameter curve (Aligizaki, 2005; Halamickova et al., 1995; Zhang and Shao, 2018). The critical diameter is interpreted as the smallest diameter of the subset of the pores that creates a connected path through the composite matrix (Berodier and Scrivener, 2015; Halamickova et al., 1995; Nishiyama and Yokoyama, 2017; Zhang and Shao, 2018), and represents the primary connected pores controlling the fluid transport behavior of the composite. The critical pore diameter decreased from approximately 30 nm in the unreacted specimens, for both WECC (Fig. 6a) and FFWECC (Fig. 6b), to < 20 nm for the control samples exposed to N_2 headspace at a temperature and pressure of 50 °C and 10 MPa. This decrease is likely due to continuous hydration and pore refinement under high temperature and pressure conditions. Similarly, carbonation of the samples due to exposure to CO_2-acidified water further decreased the critical pore diameter below 10 nm for both WECC (Fig. 6a) and FFWECC (Fig. 6b) samples. The observation that the post-carbonation critical pore diameters were comparable between the WECC and FFWECC samples indicates that the incorporation of fibers at 1.1% volume will not increase permeation of fluids through uncracked WECC.

To further understand the evolution of pore size based on the intruded volumes and differential pore size distribution curves, the total pore volume was divided into four groups based on pore diameters: voids (> 100 nm), large capillary pores (50-100 nm), medium capillary pores (10-50 nm), and gel pores (< 10 nm) (Aligizaki, 2005; Zhang and Shao, 2018). The normalized volume fraction of each group with respect to the total pore volume is shown in Fig. 7a and **b** for WECC and FFWECC, respectively. It was observed that the volume fraction of voids (pore diameter > 100 nm) doubled when PVA fibers were added to the matrix at 1.1% volume in unreacted samples (i.e., for unreacted WECC vs. unreacted FFWECC), carbonated samples, and samples exposed to N_2-headspace. In WECC samples, voids made up 34%, 33%, and 26% of the pore fraction for unreacted samples, carbonated samples, and samples exposed to N_2 headspace, respectively, while the volume fraction of voids in the FFWECC samples exposed to similar conditions was 18%, 14%, and 13%, respectively (Fig. 7**b**). This indicates that the presence of the PVA fibers coarsened the pore structure, particularly following exposure to CO_2-acidified water where the volume fraction of voids increased by over 100%.

The coarsening of the pore structure following the addition of the PVA fibers can be explained by the existence of the fiber/matrix ITZ in WECC. Analogous to the ITZ between the aggregate and cement paste in conventional concrete, a coarser pore structure is potentially created in the matrix adjacent to fibers due to the "wall effect" that accounts for the increases in the total pore volume and void fractions when the PVA

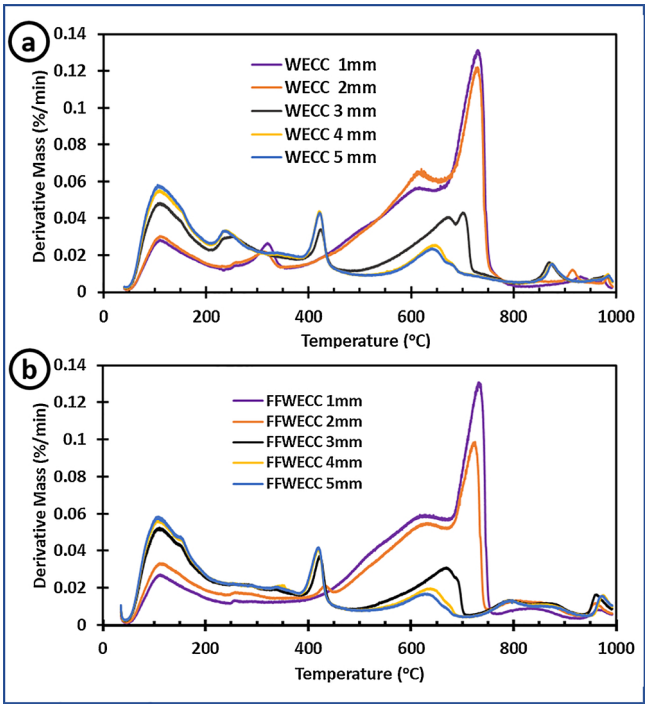

Fig. 8. DTG curves for **(a)**. WECC and **(b)**. FFWECC specimens at different depths into the carbonated coupons. The result indicates a decrease in the extent of carbonation of the samples with depth and a significantly higher extent of carbonation at the 1 to 2 mm section of the sample in comparison to the 3 to 5 mm sections. The trend and extent of carbonation for WECC and FFWECC specimens are similar. Note that the 1 mm section is the surface of the sample exposed to the solution while the 5 mm section represents the mid-section of the exposed sample.

fibers are incorporated. The volume of mercury that intruded along the ITZ is interpreted as the volume for the pore size corresponding to the percolation pressure for the ITZ width. Thus, the presence of the PVA fibers leads to an increase in the fraction of voids in WECC.

Despite the increase in the fraction of voids observed in WECC samples compared to FFWECC samples, it is interesting that the critical diameter of WECC was similar to that of FFWECC samples. This suggests that the coarsening of WECC porosity due to the presence of the ITZ is unlikely to impact the material permeability, potentially due to isolated distribution and absence of interconnectedness of the ITZ compared to the pores in the matrix. Nevertheless, further investigation is needed to understand the pore structure in WECC using direct observation techniques, such as high-resolution scanning electron microscopy coupled with backscatter electron spectroscopy and x-ray scattering, to examine how this physical change of the pore structure will impact the permeability of WECC to CO_2-rich fluids under CGS conditions.

3.6. Evolution of chemical composition

Fig. 8**a** and **b** present the derivative of thermogravimetric analysis (DTG) curves for specimens obtained at different depths along the thickness of WECC and FFWECC coupons following exposure to CO_2-acidified water for 7 days. As presented in the literature, dehydration of calcium silicate hydrate (C-S-H) occurs from 40 to 200 °C, dehydroxylation of portlandite ($Ca(OH)_2$) from 380 to 450 °C, and decarbonization of calcium carbonate ($CaCO_3$) occurs from 450 to 750 °C (Neves Junior et al., 2019, 2015; Sato et al., 2007). Material depths (measured from the outside edge of the sample) of 1 mm and 2 mm represent the fully reacted zone, the 4 mm and 5 mm sections represent the unaltered zone, and the 3 mm section is the partially carbonated zone, for both WECC and FFWECC samples (see Fig. 1**d** for schematic). The unaltered 4 mm and 5 mm sections showed comparable trends, with near overlapping DTG curves and similar magnitude for C-S-H, $Ca(OH)_2$, and $CaCO_3$. The 1 mm and 2 mm sections were depleted in $Ca(OH)_2$ but showed a significant increase in the intensity of the $CaCO_3$ peaks as compared to the unaltered sections and the transition zone, indicating the conversion of $Ca(OH)_2$ to $CaCO_3$. Similarly, the intensity of the C-S-H peak decreased progressively from the 1 mm to 5 mm section due to partial carbonation of C-S-H.

For the WECC samples, an additional peak was observed between 225 and 350 °C (Fig. 8a). This peak corresponds to the decomposition of the PVA fibers (Panaitescu et al., 2011; Peng et al., 2017; Zhou et al., 2012), which explains its absence in the FFWECC specimens. A progressive shift in the onset of thermal decomposition of PVA fibers can be clearly observed following carbonation, suggesting that the shift is a consequence of the interaction of the fibers with $CaCO_3$. This may be explained by the nucleation of $CaCO_3$ on the fibers following carbonation, as reported by Adeoye et al. (2019), which possibly led to the thermal instability of the fibers. Such shifts in the onset of thermal decomposition, relative to unmodified materials, have been reported in studies on coated fibers and fibers treated with $CaCO_3$ (Al-Sabagh et al., 2018; Bandyopadhyay-Ghosh et al., 2015; Deshmukh et al., 2010; Noor Zuhaira and Rahmah, 2013).

Fig. 9 presents the normalized percentage of $CaCO_3$ and $Ca(OH)_2$ relative to the total mass loss as a function of temperature at different depths for the WECC and FFWECC specimens. It can be seen that the $CaCO_3$ content in the specimens decreased from 41% and 42% in the most carbonated section to 5% and 7.5% in the unaltered zone for FFWECC and WECC, respectively. Similarly, the $Ca(OH)_2$ content

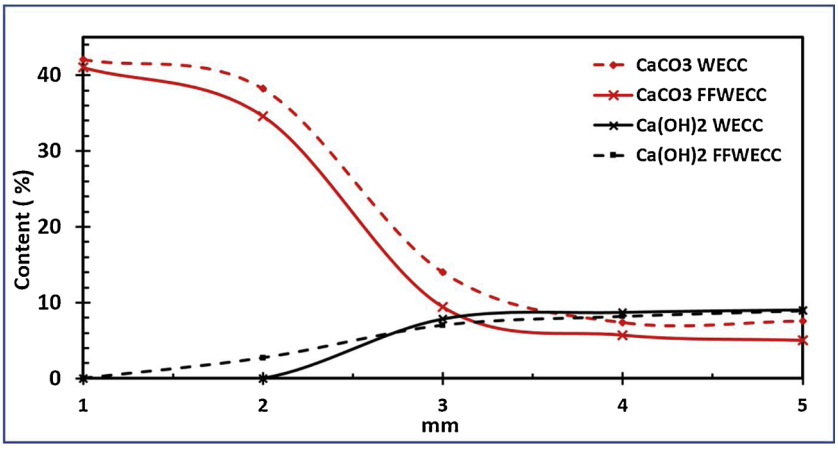

Fig. 9. Evolution of $CaCO_3$ and $Ca(OH)_2$ content in WECC and FFWECC coupons along the reaction front.

increased from 0% in the fully reacted zone to 8.9% in the unaltered zone for both FFWECC and WECC samples. Because the proportion of $Ca(OH)_2$ in unaltered cement typically varies from 15 to 20% (Michaux et al., 1990), the fact that the $Ca(OH)_2$ content in the uncarbonated core of the WECC and FFWECC was only 8.9% can be explained by depletion of the $Ca(OH)_2$ due to the pozzolanic reaction in the high-volume fly ash matrix. The most significant change in $Ca(OH)_2$ and $CaCO_3$ content occurred between the 2 mm and 3 mm sections. This mirrors the boundary of the carbonation front as determined by use of the phenolphthalein solution (Fig. 2), demonstrating that the pH indicator captured the depth of the alteration front well. The absence of sharp spikes or dips in the $CaCO_3$ content along the altered zone supports previous studies, which showed that exposure to CO_2-acidified water does not result in distinct reaction zones in fly ash-amended cementitious materials (Adeoye et al., 2019; Crow et al., 2010; Zhang et al., 2014), whereas it does in neat Portland cement (Kutchko et al., 2007). This result also shows that the presence of the fibers will not alter the chemical gradient in WECC, and its ability to protect the wellbore steel casing will not be significantly different from that of the conventional fly-ash amended wellbore cement.

4. Conclusion

In this study, a novel strain hardening engineered cementitious composite (WECC) designed for wellbore applications was exposed to CO_2-acidified water at temperature and pressure conditions of 50 °C and 10 MPa to investigate the effect of carbonation reactions on its overall mechanical integrity during GCS operations. WECC is proposed here for use in primary cementing of wellbores during GCS because it exhibits tensile ductility superior to conventional wellbore cement and has the potential to prevent damage to the cement sheath caused by stresses from casing expansion/contraction due to thermal swings during CO_2 injection. The results showed that although the tensile ductility of WECC will decrease following exposure to CO_2-acidified water, it will continue to maintain superior ductility in comparison to conventional wellbore cements under similar conditions. The incorporation of PVA fibers in WECC was found to prevent retrogression of the material hardness, which was not the case for fiber-free conventional fly ash-amended wellbore cement. It was also found that the fibers did not promote deeper depth of CO_2 penetration, as WECC exhibited similar depths of carbonation to that of conventional fly ash-amended wellbore cement at the different time points investigated. Porosity and pore size distribution analysis using MIP analysis showed that while the incorporation of fibers increased the proportion of voids in WECC, which was attributed to the presence of the fiber/matrix interface, its overall porosity and critical pore diameter trend was similar to that of fly ash-amended cement. This suggests that the fiber/matrix ITZ will not form a continuous conductive pathway and PVA fibers in WECC will not change its permeability significantly in comparison to fly ash-amended wellbore cement. Overall, the high durability exhibited by the novel fiber-reinforced WECC after exposure to CO_2-acidified water may make this material a viable candidate for wellbore cementing applications that aim to prevent cracking of the cement sheath and mitigate upward leakage of stored fluids such as supercritical CO_2.

Declaration of Competing Interest

The authors declare no financial conflict of interest.

Acknowledgement

The authors acknowledge partial funding support from the U.S. Department of Energy through grant DE-FE0030684. J. T. Adeoye received partial funding support through the University of Michigan Rackham Predoctoral Fellowship Program.

Appendix A. Supplementary data

Supplementary material related to this article can be found, in the online version, at doi:https://doi.org/10.1016/j.ijggc.2019.102896.

References

Adeoye, J.T., Beversluis, C., Murphy, A., Li, V.C., Ellis, B.R., 2019. Physical and chemical alterations in engineered cementitious composite under geologic CO2 storage conditions. Int. J. Greenh. Gas Control 83, 282–292. https://doi.org/10.1016/j.ijggc.2019.01.025.

Aligizaki, K.K., 2005. Pore Structure of Cement-Based Materials: Testing, Interpretation and Requirements. CRC Presshttps://doi.org/10.1201/9781482271959.

Al-Sabagh, A.M., Abdou, M.I., Migahed, M.A., Fadl, A.M., El-Shahat, M.F., 2018. Influence of surface modified nanoilmenite/amorphous silica composite particles on the thermal stability of cold galvanizing coating. Egypt. J. Pet. 27, 137–144. https://doi.org/10.1016/j.ejpe.2017.02.002.

ASTM, 2016. Test Method for Compressive Strength of Hydraulic Cement Mortars (Using 2-in. or [50-mm] Cube Specimens). ASTM Internationalhttps://doi.org/10.1520/C0109_C0109M-16A.

ASTM, 2012. C1609/C1609M-12. Test Method for Flexural Performance of Fiber-Reinforced Concrete (Using Beam With Third-Point Loading). ASTM Internationalhttps://doi.org/10.1520/C1609_C1609M-12.

Bachu, S., Celia, M.A., 2009. Assessing the potential for CO2 leakage, particularly through wells, from geological storage sites, in: Geophysical Monograph Series. Am. Geophys. Union Wash. C 203–216.

Bandyopadhyay-Ghosh, S., Ghosh, S.B., Sain, M., 2015. 19 - The use of biobased nanofibres in composites. In: Faruk, O., Sain, Mohini (Eds.), Biofiber Reinforcements in Composite Materials. Woodhead Publishing, pp. 571–647. https://doi.org/10.1533/9781782421276.5.571.

Barlet-Gouédard, V., Rimmelé, G., Goffé, B., Porcherie, O., 2007. Well Technologies for CO2 Geological Storage: CO2-Resistant Cement. Oil Gas Sci. Technol. - Rev. IFP 62, 325–334. https://doi.org/10.2516/ogst:2007027.

Berodier, E., Scrivener, K., 2015. Evolution of pore structure in blended systems. Cem. Concr. Res. 73, 25–35. https://doi.org/10.1016/j.cemconres.2015.02.025.

Cao, P., Karpyn, Z.T., Li, L., 2015. Self-healing of cement fractures under dynamic flow of CO2-rich brine. Water Resour. Res. 51, 4684–4701. https://doi.org/10.1002/2014WR016162.

Carroll, S., Carey, J.W., Dzombak, D., Huerta, N.J., Li, L., Richard, T., Um, W., Walsh, S.D.C., Zhang, L., 2016. Review: Role of chemistry, mechanics, and transport on well integrity in CO2 storage environments. Int J Greenh Gas Control 49, 149–160. https://doi.org/10.1016/j.ijggc.2016.01.010.

Cheshire, M.C., Stack, A.G., Carey, J.W., Anovitz, L.M., Prisk, T.R., Ilavsky, J., 2017. Wellbore Cement Porosity Evolution in Response to Mineral Alteration during CO2 Flooding. Environ. Sci. Technol. 51, 692–698. https://doi.org/10.1021/acs.est.6b03290.

Chow, J.C., Watson, J.G., Herzog, A., Benson, S.M., Hidy, G.M., Gunter, W.D., Penkala, S.J., White, C.M., 2003. Separation and Capture of CO2 from Large Stationary Sources and Sequestration in Geological Formations. J. Air Waste Manag Assoc 53, 1172–1182. https://doi.org/10.1080/10473289.2003.10466274.

Crow, W., Carey, J.W., Gasda, S., Brian Williams, D., Celia, M., 2010. Wellbore integrity analysis of a natural CO2 producer. Int. J. Greenh. Gas Control, The Ninth International Conference on Greenhouse Gas Control Technologies, vol. 4. pp. 186–197. https://doi.org/10.1016/j.ijggc.2009.10.010.

Deel, D., 2007. Carbon Sequestration Technology Roadmap and Program Plan 2007 48.

Deshmukh, G.S., Pathak, S.U., Peshwe, D.R., Ekhe, J.D., 2010. Effect of uncoated calcium carbonate and stearic acid coated calcium carbonate on mechanical, thermal and structural properties of poly(butylene terephthalate) (PBT)/calcium carbonate composites. Bull. Mater. Sci. 33, 277–284. https://doi.org/10.1007/s12034-010-0043-7.

Dieter, G.E., Bacon, D.J., 1986. Mechanical metallurgy. McGraw-hill, New York.

Fabbri, A., Corvisier, J., Schubnel, A., Brunet, F., Goffé, B., Rimmele, G., Barlet-Gouédard, V., 2009. Effect of carbonation on the hydro-mechanical properties of Portland cements. Cem 39, 1156–1163. https://doi.org/10.1016/j.cemconres.2009.07.028.

Feldman, R.F., 1987. Diffusion measurements in cement paste by water replacement using Propan-2-OL. Cem. Concr. Res. 17, 602–612. https://doi.org/10.1016/0008-8846(87)90133-5.

Gallé, C., 2001. Effect of drying on cement-based materials pore structure as identified by mercury intrusion porosimetry: A comparative study between oven-, vacuum-, and freeze-drying. Cem. Concr. Res. 31, 1467–1477. https://doi.org/10.1016/S0008-8846(01)00594-4.

Guillot, D., 1990. 4 Rheology of Well Cement Slurries. In: Nelson, E.B. (Ed.), Developments in Petroleum Science, Well Cementing. Elsevier, pp. 1–4. https://doi.org/10.1016/S0376-7361(09)70302-4.

Halamickova, P., Detwiler, R.J., Bentz, D.P., Garboczi, E.J., 1995. Water permeability and chloride ion diffusion in portland cement mortars: Relationship to sand content and critical pore diameter. Cem. Concr. Res. 25, 790–802. https://doi.org/10.1016/0008-8846(95)00069-O.

Harison, A., Srivastava, V., Herbert, A., 2014. Effect of Fly Ash on Compressive Strength of Portland Pozzolona Cement. Concrete 2, 4.

Huerta, N.J., Hesse, M.A., Bryant, S.L., Strazisar, B.R., Lopano, C., 2016. Reactive transport of CO2-saturated water in a cement fracture: Application to wellbore leakage during geologic CO2 storage. Int. J. Greenh. Gas Control 44, 276–289. https://doi.org/10.1016/j.ijggc.2015.02.006.

IPCC, Metz, B. (Eds.), 2005. IPCC special report on carbon dioxide capture and storage.

Cambridge University Press, for the Intergovernmental Panel on Climate Change, Cambridge.
Jen, C.-P., Li, C., Zhang, K., 2017. Effects of Injection Pressure on Geological CO2 Storage in the Northwest Taiwan Basin. Aerosol Air Qual. Res. 17, 1033–1042. https://doi.org/10.4209/aaqr.2016.12.0526.
Kan, Shi, -s, H., Sakulich, A.R., Li, V.C., 2010. Self-Healing Characterization of Engineered Cementitious Composite Materials. ACI Mater 107, 617–624.
Kutchko, B.G., Strazisar, B.R., Dzombak, D.A., Lowry, G.V., Thaulow, N., 2007. Degradation of Well Cement by CO2 under Geologic Sequestration Conditions. Env. Sci Technol 41, 4787–4792. https://doi.org/10.1021/es062828c.
Kutchko, B.G., Strazisar, B.R., Huerta, N., Lowry, G.V., Dzombak, D.A., Thaulow, N., 2009. CO2 Reaction with Hydrated Class H Well Cement under Geologic Sequestration Conditions: Effects of Flyash Admixtures. Env. Sci 43, 3947–3952. https://doi.org/10.1021/es803007e.
Labibzadeh, M., Zahabizadeh, B., Khajehdezfuly, A., 2010. Early-age compressive strength assessment of oil well class G cement due to borehole pressure and temperature changes 10.
Lam, L., Wong, Y.L., Poon, C.S., 1998. Effect of Fly Ash and Silica Fume on Compressive and Fracture Behaviors of Concrete. Cem. Concr. Res. 28, 271–283. https://doi.org/10.1016/S0008-8846(97)00269-X.
Li, Q., Lim, Y.M., Flores, K.M., Kranjc, K., Jun, Y.-S., 2015. Chemical Reactions of Portland Cement with Aqueous CO2 and Their Impacts on Cement's Mechanical Properties under Geologic CO2 Sequestration Conditions. Env. Sci Technol 49, 6335–6343. https://doi.org/10.1021/es5063488.
Li, V., Wu, C., Wang, S., Ogawa, A., Saito, T., 2002. Interface Tailoring for Strain-Hardening Polyvinyl Alcohol-Engineered Cementitious Composite (PVA-ECC). ACI Mater. J. 99. https://doi.org/10.14359/12325.
Li, V.C., 2009. Engineered Cementitious Composites (ECC) – material, structural and durability performance. Concrete Construction Engineering Handbook. CRC Press, Boca Raton.
Li, V.C., 2003. On engineered cementitious composites (ECC). J Adv 1, 215–230.
Lye, C.-Q., Dhir, R.K., Ghataora, G.S., 2015. Carbonation resistance of fly ash concrete. Mag. Concr. Res. 67, 1150–1178. https://doi.org/10.1680/macr.15.00204.
Michaux, M., Nelson, E.B., Vidick, B., 1990. 2 Chemistry and Characterization of Portland Cement. In: Nelson, E.B. (Ed.), Developments in Petroleum Science, Well Cementing. Elsevier, pp. 1–2. https://doi.org/10.1016/S0376-7361(09)70300-0.
Mohamed, M., Li, V.C., 1994. Flexural/Tensile-Strength Ratio in Engineered Cementitious Composites. J. Mater. Civ. Eng. 6, 513–528. https://doi.org/10.1061/(ASCE)0899-1561(1994)6:4(513).
Nelson, E.B., 1990. Well Cementing. Newnes.
Nelson, E.B., Baret, J.-F., Michaux, M., 1990. 3 Cement Additives and Mechanisms of Action. In: Nelson, E.B. (Ed.), Developments in Petroleum Science, Well Cementing. Elsevier, pp. 1–3. https://doi.org/10.1016/S0376-7361(09)70301-2.
Neves Junior, A., Dweck, J., Filho, R.D.T., Ellis, B., Li, V., 2019. Determination of CO2 capture during accelerated carbonation of engineered cementitious composite pastes by thermogravimetry. J. Therm. Anal. Calorim. https://doi.org/10.1007/s10973-019-08210-y.
Junior, Neves, A, Toledo Filho, R.D, de Moraes Rego, Fairbairn, E., Dweck, J., 2015. The effects of the early carbonation curing on the mechanical and porosity properties of high initial strength Portland cement pastes. Constr. Build. Mater. 77, 448–454. https://doi.org/10.1016/j.conbuildmat.2014.12.072.
Neville, A.M., 2011. Properties of concrete, 5th ed. Pearson, Harlow, England; New York.
Nishiyama, N., Yokoyama, T., 2017. Permeability of porous media: Role of the critical pore size. J. Geophys. Res. Solid Earth 122, 6955–6971. https://doi.org/10.1002/2016JB013793.
Noor Zuhaira, A.A., Rahmah, M., 2013. Effect of Calcium Carbonate on Thermal Properties of $CaCO_3$/Kenaf/HDPE and $CaCO_3$/Rice Husk/HDPE Composites. Adv. Mater. Res. 812, 175–180. https://doi.org/10.4028/www.scientific.net/AMR.812.175.
Nordbotten, J.M., Celia, M.A., Bachu, S., Dahle, H.K., 2005. Semianalytical Solution for CO2 Leakage through an Abandoned Well. Environ. Sci. Technol. 39, 602–611. https://doi.org/10.1021/es035338i.
Nordbotten, J.M., Kavetski, D., Celia, M.A., Bachu, S., 2009. Model for CO2 Leakage Including Multiple Geological Layers and Multiple Leaky Wells. Environ. Sci. Technol. 43, 743–749. https://doi.org/10.1021/es801135v.
Panaitescu, D., Frone, A., Ghiurea, M., Spataru, C., Radovici, C., Iorga, M., 2011. Properties of Polymer Composites with Cellulose Microfibrils, in: Advances in Composite Materials: Ecodesign and Analysis. BoD – Books on Demand.
Peng, S., Zhou, M., Liu, F., Zhang, C., Liu, X., Liu, J., Zou, L., Chen, J., 2017. Flame-retardant polyvinyl alcohol membrane with high transparency based on a reactive phosphorus-containing compound. R. Soc. Open Sci. 4, 170512. https://doi.org/10.1098/rsos.170512.
Redon, C., Li, V.C., Wu, C., Hoshiro, H., Saito, T., Ogawa, A., 2001. Measuring and Modifying Interface Properties of PVA Fibers in ECC Matrix. J. Mater. Civ. Eng. 13, 399–406. https://doi.org/10.1061/(ASCE)0899-1561(2001)13:6(399).
Ridha, S., Irawan, S., Ariwahjoedi, B., 2013. Strength prediction of Class G oilwell cement during early ages by electrical conductivity. J. Pet. Explor. Prod. Technol. 3, 303–311. https://doi.org/10.1007/s13202-013-0075-9.
RILEM, 1984. CPC-18 Measurement of hardened concrete carbonation depth.
Rimmelé, G., Barlet-Gouédard, V., Porcherie, O., Goffé, B., Brunet, F., 2008. Heterogeneous porosity distribution in Portland cement exposed to CO2-rich fluids. Cem. Concr. Res. 38, 1038–1048. https://doi.org/10.1016/j.cemconres.2008.03.022.
Roy, P., Morris, J.P., Walsh, S.D.C., Iyer, J., Carroll, S., 2018. Effect of thermal stress on wellbore integrity during CO2 injection. Int. J. Greenh. Gas Control 77, 14–26. https://doi.org/10.1016/j.ijggc.2018.07.012.
Rutqvist, J., Birkholzer, J., Cappa, F., Tsang, C.-F., 2007. Estimating maximum sustainable injection pressure during geological sequestration of CO2 using coupled fluid flow and geomechanical fault-slip analysis. Energy Convers. Manag. 48, 1798–1807. https://doi.org/10.1016/j.enconman.2007.01.021.
Sato, T., Beaudoin, J.J., Ramachandran, V.S., Mitchell, L.D., Tumidajski, P.J., 2007. Thermal decomposition of nanoparticulate Ca(OH)2-anomalous effects. Adv. Cem. Res. 19, 1–7. https://doi.org/10.1680/adcr.2007.19.1.1.
Spycher, N., Pruess, K., 2005. CO2-H2O mixtures in the geological sequestration of CO2. II. Partitioning in chloride brines at 12–100°C and up to 600 bar. Geochim. Cosmochim. Acta 69, 3309–3320. https://doi.org/10.1016/j.gca.2005.01.015.
Verbeck, G., 1958. Carbonation of Hydrated Portland Cement. Committee C-1, Committee C-9 (Eds.), Cement and Concrete. ASTM International, 100 Barr Harbor Drive, PO Box C700, West Conshohocken, PA 19428-2959, pp. 17-17–20. https://doi.org/10.1520/STP39460S.
Watson, T.L., Bachu, S., 2009. Evaluation of the Potential for Gas and CO2 Leakage Along Wellbores. SPE Drill 24, 115–126. https://doi.org/10.2118/106817-PA.
Wu, H.-L., Zhang, D., Ellis, B.R., Li, V.C., 2018. Development of reactive MgO-based Engineered Cementitious Composite (ECC) through accelerated carbonation curing. Constr. Build. Mater. 191, 23–31. https://doi.org/10.1016/j.conbuildmat.2018.09.196.
Zhang, D., Shao, Y., 2018. Surface scaling of CO2-cured concrete exposed to freeze-thaw cycles. J. CO2 Util. 27, 137–144. https://doi.org/10.1016/j.jcou.2018.07.012.
Zhang, D., Shao, Y., 2016. Early age carbonation curing for precast reinforced concretes. Constr. Build. Mater. 113, 134–143. https://doi.org/10.1016/j.conbuildmat.2016.03.048.
Zhang, L., Dzombak, D.A., Nakles, D.V., Hawthorne, S.B., Miller, D.J., Kutchko, B.G., Lopano, C.L., Strazisar, B.R., 2014. Rate of H2S and CO2 attack on pozzolan-amended Class H well cement under geologic sequestration conditions. Int. J. Greenh. Gas Control 27, 299–308. https://doi.org/10.1016/j.ijggc.2014.02.013.
Zhang, L., Dzombak, D.A., Nakles, D.V., Hawthorne, S.B., Miller, D.J., Kutchko, B.G., Lopano, C.L., Strazisar, B.R., 2013. Characterization of pozzolan-amended wellbore cement exposed to CO2 and H2S gas mixtures under geologic carbon storage conditions. Int. J. Greenh. Gas Control 19, 358–368. https://doi.org/10.1016/j.ijggc.2013.09.004.
Zhang, P., Li, Q.-F., 2013. Combined effect of polypropylene fiber and silica fume on workability and carbonation resistance of concrete composite containing fly ash. Proc. Inst. Mech. Eng. Part J. Mater. Des. Appl. 227, 250–258. https://doi.org/10.1177/1464420712458198.
Zhou, K., Jiang, S., Bao, C., Song, L., Wang, B., Tang, G., Hu, Y., Gui, Z., 2012. Preparation of poly(vinyl alcohol) nanocomposites with molybdenum disulfide (MoS 2): structural characteristics and markedly enhanced properties. RSC Adv. 2, 11695–11703. https://doi.org/10.1039/C2RA21719H.